Biomaterials

DOI: 10.1002/anie.201409050

Influence of the β-Sheet Content on the Mechanical Properties of Aggregates during Amyloid Fibrillization**

Francesco Simone Ruggeri, Jozef Adamcik, Jae Sun Jeong, Hilal A. Lashuel, Raffaele Mezzenga, and Giovanni Dietler**

Abstract: *Amyloid fibrils associated with neurodegenerative diseases, such as Parkinson's and Alzheimer's, consist of insoluble aggregates of α-synuclein and Aβ-42 proteins with a high β-sheet content. The aggregation of both proteins occurs by misfolding of the monomers and proceeds through the formation of intermediate oligomeric and protofibrillar species to give the final fibrillar cross-β-sheet structure. The morphological and mechanical properties of oligomers, protofibrils, and fibrils formed during the fibrillization process were investigated by thioflavin T fluorescence and circular dichroism in combination with AFM peak force quantitative nanomechanical technique. The results reveal an increase in the Young's modulus during the transformation from oligomers to mature fibrils, thus inferring that the difference in their mechanical properties is due to an internal structural change from a random coil to a structure with increased β-sheet content.*

Amyloid fibrils are highly ordered insoluble protein aggregates. They are most often related to human diseases, including numerous neurodegenerative disorders, such as Parkinson's disease and Alzheimer's disease.[1–3] However, amyloid fibrils have also been discovered in many physiologically beneficial roles, including bacterial coatings, catalytic scaffolds, adhesives, and structures for the storage of peptide hormones.[4–6] For amyloid fibrils in such roles, the term functional amyloids has been cast. A characteristic fingerprint of amyloid fibrils is the core cross-β-sheet structure, in which β-strands contained within the β-sheets are oriented perpendicular to the fibril axis.[7–10] Moreover, amyloid fibrils exhibit remarkable mechanical properties with Young's moduli in the range of several gigapascals.[11–14] Inspiration from functional amyloids and the self-assembly of nontoxic proteins and peptides in vitro into highly ordered structures with unique mechanical properties has led to the development of biomaterials for a broad spectrum of applications in medicine, food, and nanotechnology.[15–19]

Experimental techniques, such as atomic force microscopy (AFM), and computational simulations have been widely used to quantify the mechanical properties of amyloid fibrils. AFM is one of the most suitable methods for quantitative measurements of the local elasticity of amyloid fibrils. AFM single-molecule-imaging features combined with the statistical analysis of AFM images,[12,20,21] together with the possibility of imposing and measuring forces,[11,22] make AFM a particularly useful research tool that can ideally deliver important information about the mechanical and related structural properties of amyloid fibrils at the single-molecule scale. Atomistic simulations performed by Buehler and coworkers have also provided theoretical values of the Young's moduli of amyloid fibrils of the order of several gigapascals.[23–28] Moreover, the results obtained by both AFM and simulations suggest that the intermolecular interactions (e.g. hydrogen bonds) between β-sheet layers are responsible for the remarkable mechanical properties of amyloid fibrils. Recently, a relatively new AFM technique known as peak force quantitative nanomechanical mapping (PF-QNM) has been used to estimate the values of the Young's moduli of different classes of mature amyloid fibrils in the gigapascal range.[29–32] The results are consistent with the values of the Young's moduli obtained by statistical analysis of AFM images.[12,29]

To appreciate the full potential of amyloid fibrils as biomaterials, it is important to understand the mechanism of the fibrillization process and to measure and quantify the mechanical properties of amyloid fibrils. Moreover, understanding of the mechanical properties and intermediate structures during the fibrillization process is of fundamental importance for the elucidation of the stability, toxicity, and mechanism of clearance of amyloid fibrils so that new therapeutic strategies can be designed to combat the onset of neurodegenerative disorders. In this study, we investigated the evolution of both the mechanical and structural properties of amyloidogenic structures formed throughout the fibrillization process of α-synuclein and Aβ(1–42) (Aβ-42).

The typical methods used to study the kinetics of amyloid fibrillization and to investigate the structural change that the proteins undergo during the fibrillization process are thio-

[*] F. S. Ruggeri,[+] J. S. Jeong, Prof. G. Dietler
Laboratory of Physics of Living Matter
Ecole Polytechnique Fédérale de Lausanne (EPFL)
Route de la Sorge, 1015 Lausanne (Switzerland)
E-mail: giovanni.dietler@epfl.ch

Dr. J. Adamcik,[+] Prof. R. Mezzenga
Food and Soft Materials Science, Institute of Food, Nutrition and Health, Department of Health Sciences and Technology, ETH Zürich
Schmelzbergstrasse 9, LFO E23, 8092, Zürich (Switzerland)
E-mail: raffaele.mezzenga@hest.ethz.ch

Prof. H. A. Lashuel
Laboratory of Molecular and Chemical Biology of Neurodegeneration, Brain Mind Institute
Ecole Polytechnique Fédérale de Lausanne (EPFL)
1015 Lausanne (Switzerland)

[+] These authors contributed equally.

[**] We thank the Swiss National Foundation for Science for financial support (Project Number 152958).

Supporting information for this article is available on the WWW under http://dx.doi.org/10.1002/anie.201409050.

flavin T (ThT) fluorescence[33] and circular dichroism (CD),[34] respectively. We carried out ThT and CD measurements during the fibrillization of α-synuclein (Figure 1 a,c) and Aβ-42 (Figure 1 b,d).

Amyloid-fibril formation, as monitored by ThT, is generally characterized by a sigmoidal curve representing three main steps of the fibrillization process: an initial lag phase, during which monomers misfold and oligomeric nuclei form; fast exponential growth due to the fast formation/elongation of protofibrillar and fibrillar structures; and a plateau indicating a dynamic equilibrium within the final mature amyloid fibrils. The fibrillization processes of both α-synuclein and Aβ-42 followed the usually described sigmoid curve attributed to a nucleation-dependent polymerization process (Figure 1 a,b).[35,36] The fibrillization process of α-synuclein was slower than that of Aβ-42 because even after incubation for 24 days, the ThT signal did not reach the plateau phase and was increasing as a function of time after the exponential phase (Figure 1 a), thus suggesting that the fibrils were still forming/elongating. In the fibrillization of Aβ-42, the ThT signal reached the plateau region after only 30 h, and fibril formation remained in a stationary dynamic equilibrium (Figure 1 b).

CD spectra of α-synuclein fibrillization (Figure 1 c) showed a peak minimum at 203 nm corresponding to a random-coil structure at 0 h, whereas after incubation for 48 h, the peak minimum was shifted to 220 nm, thus indicating the formation of the β-sheet structure. The intensity of the CD signal at 220 nm increased as a function of time and, according to the ThT signal, also as a function of fibril formation. In the case of Aβ-42 fibrillization (Figure 1 d), the peak minimum at 0 h was detected at 195 nm, thus indicating a random-coil structure, whereas after incubation for 24 h, the peak minimum was shifted to 218 nm, thus indicating the presence of the β-sheet structure. In this case, the intensity of the CD signal at 218 nm decreased as a function of time. Since the kinetics of Aβ-42 fibril formation had already reached the stationary regime after incubation for 30 h according to the ThT results (Figure 1 b), and amyloids are insoluble aggregates, sedimentation, which occurs during the measurements, can explain the decrease in the intensity of the CD signal, as evidenced by the turbidity of the solution. This trend, together with the slow aggregation kinetics, which leads to coexistence of unfolded oligomers with growing fibrils, complicates the evaluation of the exact composition of β-sheets in the protofibrils during fibrillization, although it is evident from Figure 1 that both systems evolve towards an overall increase in β-sheet structureduring aggregation.

Amyloid fibrillization is a complex process that proceeds through multiple pathways, and several polymorphic amyloid species are present simultaneously in the heterogeneous solution during aggregation.[37] For this reason, bulk techniques, such as ThT fluorescence and CD, only provide averaged information about this ensemble. A single-molecule technique, such as AFM, enables information to be gained on the fibrillization process and on individual protein structural transitions.[12,20,22] AFM images taken during the fibrillization of α-synuclein and Aβ-42 are displayed in Figure 2. At 0 h, α-synuclein was mainly in the monomeric form, since the CD spectrum showed the typical random-coil signal of intrinsically disordered proteins, and few early oligomers were observed in the AFM morphology image (Figures 1 a and 2 a;

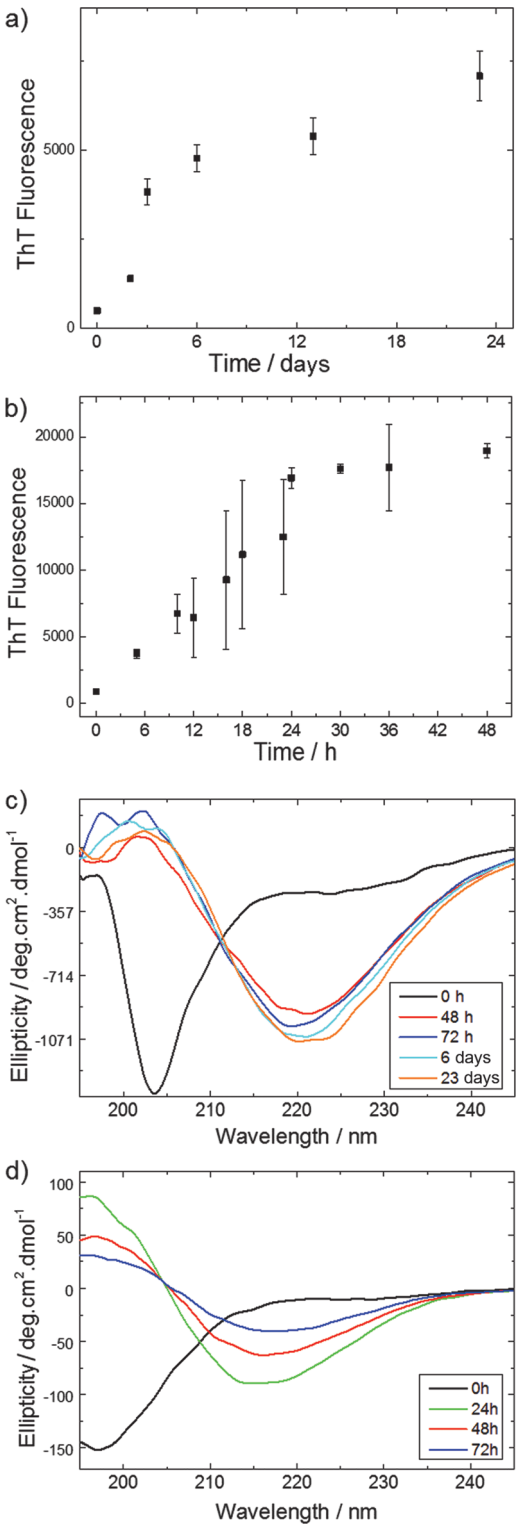

Figure 1. Kinetics of amyloid-fibril formation and secondary-structure measurements. a, b) Thioflavin T fluorescence of α-synuclein (a) and Aβ-42 (b). c, d) Circular dichroism measurements of α-synuclein (c) and Aβ-42 (d). Measurements were conducted at a concentration of 45 μM for α-synuclein and 20 μM for Aβ-42.

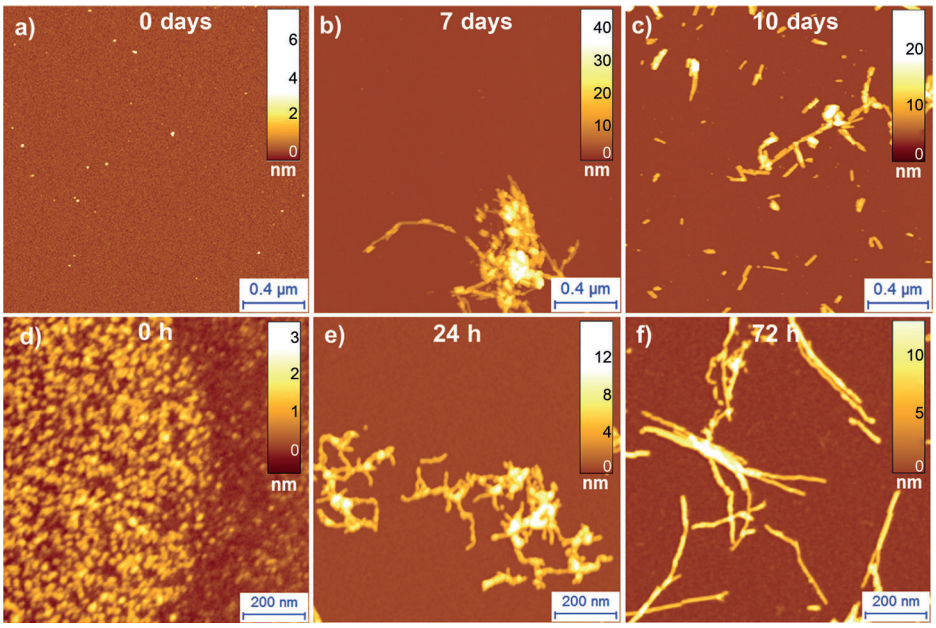

Figure 2. AFM imaging of the α-synuclein and Aβ-42 fibrillization process at incubation times of: a) 0 days, b) 7 days, and c) 10 days for α-synuclein; and d) 0 h, e) 24 h, and f) 72 h for Aβ-42.

see also Figure S1 in the Supporting Information). Already after an incubation period of 24 h, an increase in the number of bigger oligomers, with heights of 2–6 nm, was detected (see Figure S2). After incubation for 7 days, the fibrillar structures started to assemble (Figure 2b) and then continued to form mature amyloid fibrils (Figure 2c), which had a height of 6–7 nm (see Figure S3) at an incubation time of 10 days. Similarly to the case of α-synuclein, Aβ-42 was present in monomeric and early oligomeric structures (Figures 1d and 2d) with a height of 0.5–3 nm at 0 h (see Figure S4). After incubation for 24 h, abundant curly protofibrillar structures (Figure 2e) with a height of 3–4 nm were observed (see Figure S5). Finally, at an incubation time of 72 h, mature amyloid fibrils (Figure 2f) with a height of 4–6 nm had formed (see Figure S6). Thus, for both proteins, the classical oligomerization process of aggregation[35,38] was observed.

To characterize the mechanical properties of the different species formed during the fibrillization process, we performed PF-QNM measurements. The mechanical properties of α-synuclein early oligomeric structures formed at 24 h and mature fibrils formed at 10 days were investigated (Figure 3). A Young's modulus of (1.5 ± 0.5) GPa was found for oligomers (Figure 3e), whereas the measured value of the Young's modulus for fibrils was (2.2 ± 0.6) GPa (Figure 3f), which is in agreement with previously reported results, available for mature fibrils only.[30,32] To rule out a surface effect on the estimation of the Young's modulus, the fibrillization of α-synuclein was studied by AFM imaging on two other substrates: positively functionalized APTES-mica and hydrophobic highly ordered pyrolitic graphite (HOPG) (see Figure S7). The value of the Young's modulus of fibrils adsorbed on these two substrates was (2.2 ± 0.6) GPa (Figure 3g,h), thus demonstrating that PF-QNM measurements

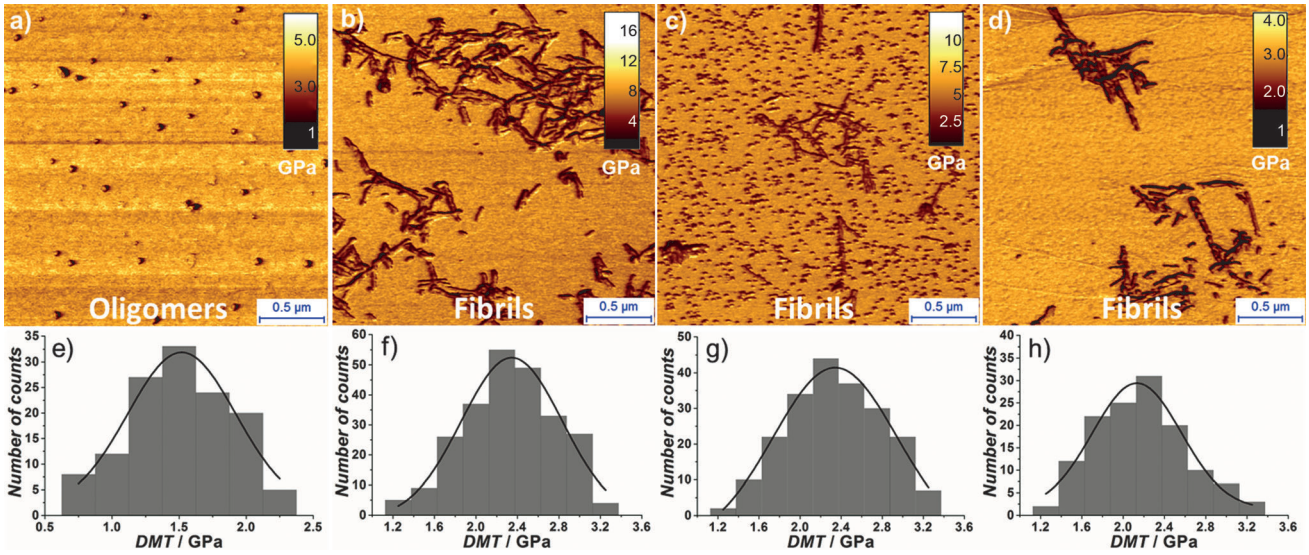

Figure 3. Evolution of the Young's modulus of α-synuclein during the fibrillization process. a–d) Derjaguin–Mueller–Toporov (DMT) modulus AFM images of oligomers on APTES-mica at an incubation time of 24 h (a) and of fibrils at an incubation time of 10 days on APTES-mica (b), mica (c), and highly ordered pyrolytic graphite (HOPG; d). e–h) Distribution of the Young's modulus of oligomers on APTES-mica (e) and of fibrils on APTES-mica (f), mica (g), and HOPG (h).

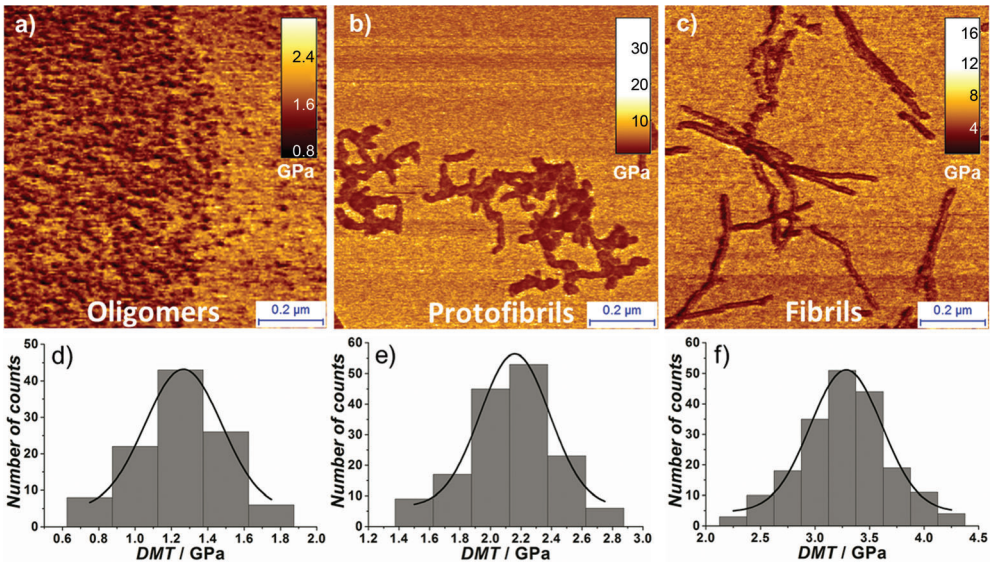

Figure 4. Evolution of the Young's modulus of Aβ-42 during the fibrillization process. a) DMT-modulus AFM images of oligomers at 0 h (a), protofibrils at 48 h (b), and fibrils at 72 h (c). d–f) Distribution of the measured Young's modulus for oligomers (d), protofibrils (e), and fibrils (f).

are independent of surface influences. Moreover, the nanoindentation measurements were validated on thick aggregates of α-synuclein (> 50 nm), in which corrections for both the substrate and the cantilever-tip radius become irrelevant; the results obtained were identical to those for single-fibril indentation, within experimental error (see Figure S8). Finally, oligomers possess a lower elastic modulus than mature fibrils, but still of the order of gigapascals.

To generalize these results, we also performed PF-QNM measurements for Aβ-42 fibrillization (Figure 4). The Young's modulus of the oligomers (Figure 4a), protofibrils (Figure 4b), and mature fibrils (Figure 4c) was evaluated accordingly. As in the case of α-synuclein, the value of the Young's modulus increased from a value of (1.2 ± 0.5) GPa for oligomers (Figure 4d) to (2.1 ± 0.6) GPa for protofibrils (Figure 4e) and a final value of (3.3 ± 0.8) GPa for mature fibrils (Figure 4f). Once again, oligomers and protofibrils showed an increasing and high value of intrinsic stiffness of the order of gigapascals, but still lower than that of mature fibrils. Indeed, we suggest the generality of this result, since we previously found that the stiffness value of several mature amyloid fibrils ranged from 2 to 4 GPa (see Table S1 in the Supporting Information).

It was mentioned above that the hydrogen bonds between β-sheets play a key role in determining the mechanical properties of amyloid fibrils, and the presence of β-sheets is a characteristic feature of amyloid fibrils. It has also been reported that during the aggregation process, oligomers or protofibrils that may be present contain partial β-sheet conformations.[39] Thus, it is thought that the β-sheet content of the structures assembled during the fibrillization process is an important parameter that affects the mechanical properties of these structures. The presented results confirm these predictions. Indeed, although mature fibrils were initially not observed by AFM, CD spectra already indicated the presence of β-sheet structures at 48 h for α-synuclein (Figure 1c) and 24 h for Aβ-42 (Figure 1d), and the measured values of the Young's moduli of the corresponding assembled structures (oligomers and protofibrillar structures) were already of the order of gigapascals (Figures 3 and 4).

In conclusion, the increase in the Young's modulus during amyloid fibrillization can be interpreted as the result of the internal structural rearrangement of monomers from their intrinsically disordered structure towards aggregated structures containing an increasing β-sheet conformation. The quantitative understanding provided by this study in terms of the structural and mechanical properties of α-synuclein and Aβ-42 aggregate snapshots during the fibrillization process could be of great significance for the elucidation of the cytotoxicity mechanisms of Parkinson's and Alzheimer's diseases and the design of new therapeutic strategies.

Received: September 12, 2014
Revised: November 28, 2014
Published online: January 14, 2015

Keywords: amyloids · mechanical properties · nanomaterials · neurodegenerative disorders · scanning probe microscopy

[1] B. Caughey, P. T. Lansbury, *Annu. Rev. Neurosci.* **2003**, *26*, 267–298.
[2] C. M. Dobson, *Nature* **2003**, *426*, 884–890.
[3] F. Chiti, C. M. Dobson, *Annu. Rev. Biochem.* **2006**, *75*, 333–366.
[4] M. R. Chapman, L. S. Robinson, J. S. Pinkner, R. Roth, J. Heuser, M. Hammar, S. Normark, S. J. Hultgren, *Science* **2002**, *295*, 851–855.
[5] D. M. Fowler, A. V. Koulov, W. E. Balch, J. W. Kelly, *Trends Biochem. Sci.* **2007**, *32*, 217–224.
[6] F. Shewmaker, R. P. McGlinchey, R. B. Wickner, *J. Biol. Chem.* **2011**, *286*, 16533–16540.
[7] M. Sunde, L. C. Serpell, M. Bartlam, P. E. Fraser, M. B. Pepys, C. C. Blake, *J. Mol. Biol.* **1997**, *273*, 729–739.
[8] R. Nelson, M. R. Sawaya, M. Balbirnie, A. Ø. Madsen, C. Riekel, R. Grothe, D. Eisenberg, *Nature* **2005**, *435*, 773–778.
[9] A. W. P. Fitzpatrick, G. T. Debelouchina, M. J. Bayro, D. K. Clare, M. A. Caporini, V. S. Bajaj, C. P. Jaroniec, L. Wang, V. Ladizhansky, S. A. Müller, C. E. MacPhee, C. A. Waudby, H. R. Mott, A. De Simone, T. P. J. Knowles, H. R. Saibil, M. Vendruscolo, E. V. Orlova, R. G. Griffin, C. M. Dobson, *Proc. Natl. Acad. Sci. USA* **2013**, *110*, 5468–5473.
[10] J. Adamcik, R. Mezzenga, *Macromolecules* **2012**, *45*, 1137–1150.

[11] J. F. Smith, T. P. Knowles, C. M. Dobson, C. E. Macphee, M. E. Welland, *Proc. Natl. Acad. Sci. USA* **2006**, *103*, 15806 – 15811.
[12] T. P. Knowles, A. W. Fitzpatrick, S. Meehan, H. R. Mott, M. Vendruscolo, C. M. Dobson, M. E. Welland, *Science* **2007**, *318*, 1900 – 1903.
[13] T. P. Knowles, M. J. Buehler, *Nat. Nanotechnol.* **2011**, *6*, 469 – 479.
[14] A. W. Fitzpatrick, S. T. Park, A. H. Zewail, *Proc. Natl. Acad. Sci. USA* **2013**, *110*, 10976 – 10981.
[15] C. Li, J. Adamcik, R. Mezzenga, *Nat. Nanotechnol.* **2012**, *7*, 421 – 427.
[16] T. P. Knowles, T. W. Oppenheim, A. K. Buell, D. Y. Chirgadze, M. E. Welland, *Nat. Nanotechnol.* **2010**, *5*, 204 – 207.
[17] S. Ling, C. Li, J. Adamcik, Z. Shao, X. Chen, R. Mezzenga, *Adv. Mater.* **2014**, *26*, 4569 – 4574.
[18] I. Cherny, E. Gazit, *Angew. Chem. Int. Ed.* **2008**, *47*, 4062 – 4069; *Angew. Chem.* **2008**, *120*, 4128 – 4136.
[19] L. Adler-Abramovich, N. Kol, I. Yanai, D. Barlam, R. Z. Shneck, E. Gazit, I. Rousso, *Angew. Chem. Int. Ed.* **2010**, *49*, 9939 – 9942; *Angew. Chem.* **2010**, *122*, 10135 – 10138.
[20] J. Adamcik, J. M. Jung, J. Flakowski, P. De Los Rios, G. Dietler, R. Mezzenga, *Nat. Nanotechnol.* **2010**, *5*, 423 – 428.
[21] A. Relini, S. Torrassa, R. Ferrando, R. Rolandi, S. Campioni, F. Chiti, A. Gliozzi, *Biophys. J.* **2010**, *98*, 1277 – 1284.
[22] J. Adamcik, R. Mezzenga, *Curr. Opin. Colloid Interface Sci.* **2012**, *17*, 369 – 376.
[23] Z. Xu, R. Paparcone, M. J. Buehler, *Biophys. J.* **2010**, *98*, 2053 – 2062.
[24] R. Paparcone, M. J. Buehler, *Biomaterials* **2011**, *32*, 3367 – 3374.
[25] R. Paparcone, S. Keten, M. J. Buehler, *J. Biomech.* **2010**, *43*, 1196 – 1201.
[26] R. Paparcone, S. W. Cranford, M. J. Buehler, *Nanoscale* **2011**, *3*, 1748 – 1755.
[27] M. Solar, M. J. Buehler, *J. Mech. Behav. Biomed. Mater.* **2013**, *19*, 43 – 49.
[28] M. Solar, M. J. Buehler, *Nanotechnology* **2014**, *25*, 105703.
[29] J. Adamcik, A. Berquand, R. Mezzenga, *Appl. Phys. Lett.* **2011**, *98*, 193701.
[30] J. Adamcik, C. Lara, I. Usov, J. S. Jeong, F. S. Ruggeri, G. Dietler, H. A. Lashuel, I. W. Hamley, R. Mezzenga, *Nanoscale* **2012**, *4*, 4426 – 4429.
[31] C. Lara, S. Gourdin-Bertin, J. Adamcik, S. Bolisetty, R. Mezzenga, *Biomacromolecules* **2012**, *13*, 4213 – 4221.
[32] K. Sweers, K. van der Werf, M. Bennink, V. Subramaniam, *Nanoscale Res. Lett.* **2011**, *6*, 270.
[33] L. Giehm, N. Lorenzen, D. E. Otzen, *Methods* **2011**, *53*, 295 – 305.
[34] M. Calero, M. Gasset, *Methods Mol. Biol.* **2012**, *849*, 53 – 68.
[35] A. L. Fink, *Acc. Chem. Res.* **2006**, *39*, 628 – 634.
[36] J. S. Jeong, A. Ansaloni, R. Mezzenga, H. A. Lashuel, G. Dietler, *J. Mol. Biol.* **2013**, *425*, 1765 – 1781.
[37] J. S. Pedersen, C. B. Andersen, D. E. Otzen, *FEBS J.* **2010**, *277*, 4591 – 4601.
[38] C. Haass, D. J. Selkoe, *Nat. Rev. Mol. Cell Biol.* **2007**, *8*, 101 – 112.
[39] D. Hong, S. Han, A. L. Fink, V. N. Uversky, *Protein Pept. Lett.* **2011**, *18*, 230 – 240.

